

# EXAMPLES OF PIV APPLICATIONS TO SUBSONIC FLOWS

**G.G. Gadzhimagomedov, V.A. Vlasov, V.M. Lutovinov**  
*Central Aerohydrodynamic Institute*

**Keywords:** *wind tunnel, PIV system, aerodynamic loads, lift coefficient, drag coefficient*

## Abstract

*An assessment of applicability of using PIV-velocity data for the nonintrusive aerodynamic force characterization (lift and drag) of an airfoil is made. The method of the control volume based on integration of hydrodynamic variables along the closed contour around an airfoil was used for calculations. The results of these calculations were compared with results of standard pressure-based lift coefficient measurements (surface pressure distribution and wake rake).*

## 1 Introduction

It is convenient to study the characteristics of the flow around components that can be considered two dimensional, such as aircraft wings, propeller blades, or turbine airfoils, using optical methods for measurements of flow characteristics in a certain section. These include, in particular, a method of velocity field detection by the particle images [particle image velocimetry, (PIV)]. PIV is a convenient and powerful tool for flow diagnostics in wind tunnels, allowing to obtain instantaneous velocity fields in whole regions and thereby to detect and evaluate the instantaneous spatial flow structures. At a sufficient spatial resolution the instantaneous spatial derivatives can be calculated based on the results of PIV measurements. This is a significant advantage compared to the conventional methods of probe technique measurements.

The ability to measure the instantaneous flow velocity field in a certain section makes it theoretically possible to use PIV in studying airfoil aerodynamic forces acting on a two-dimensional streamlined configuration, which is

an important objective in the design of such aircraft components. There are some papers in which, in order to obtain the forces acting on an object in the flow, the results of optical measurements of the velocity fields were used [1,2]. In [1] the local aerodynamic forces acting on the propeller blades of the helicopter were studied, and the method of laser Doppler anemometry was used to measure the velocity field. The study object in [2] was the airfoil, the velocity field around which was measured by PIV. The optical methods of measuring local aerodynamic forces become a particularly useful tool in experiments, where for whatever reasons the use of traditional methods is associated with some difficulties. For example, in tests with small size models, it is technically difficult to construct pressure taps system with acceptable spatial resolution. Also pressure taps measurements of aerodynamic forces acting on the helicopter rotor blades can be referred to as technically difficult.

This paper presents the results of PIV studies of aerodynamic forces acting on a wing airfoil. The tests were performed at a Reynolds number  $Re = 2 \times 10^5$  based on the length of the airfoil chord. Calculation of aerodynamic forces of the airfoil based on the velocity field at low Reynolds numbers has the advantage over the standard surface pressure distribution measurements, which become extremely unreliable and difficult to implement when reducing the model size and flow rate, while for the PIV method of measuring the velocity fields, the given conditions do not lead to reducing the accuracy due to the possibility of changing the parameters of the experiment: optical zoom and interframe delay.

## 2 Technique

The present technique allows to obtain integral aerodynamic forces acting on an object in the flow by integrating gas dynamics variables (velocity  $u$ , pressure  $p$ , density  $\rho$ , Reynolds stress tensor  $\tau$ ) over the control surface around the object (control volume method; see Fig. 1).

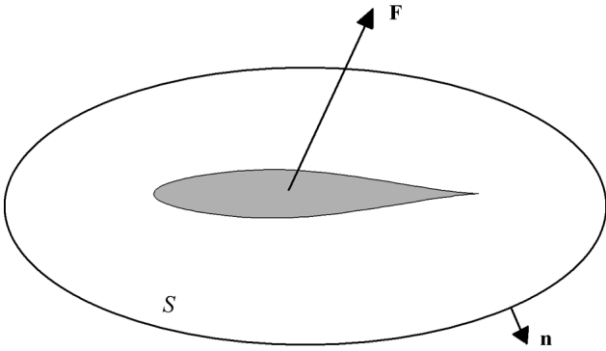


Fig. 1. Scheme of the aerodynamic forces measurement for two-dimensional airfoil flow.

If we assume the flow to be incompressible and the viscosity constant, the application of this method requires information about the velocity field in the region surrounded by the control surface, and also the pressure distribution on it. The optical system allows measuring the velocity field, and the pressure distribution can be obtained using a finite difference approximation of the Navier-Stokes equations:

$$-\frac{\partial p}{\partial x_i} = \rho u_j \frac{\partial u_i}{\partial x_j} - \mu \frac{\partial^2 u_i}{\partial x_j \partial x_j} \quad (1)$$

In the present study the PIV system configuration with a small resolution in time (1.25 Hz) was used, so the time-averaged velocity fields and the averaged forces, calculated correspondingly, were studied. For such a problem formulation, the aerodynamic force can be obtained using the momentum conservation law for a steady flow, integrating the expression

$$\mathbf{F} = \iint_S (\tau - p\mathbf{I} - \rho\mathbf{u}\mathbf{u}) \cdot \mathbf{n} dS, \quad (2)$$

$$\tau_{ij} = \mu \left( \frac{\partial u_i}{\partial x_j} + \frac{\partial u_j}{\partial x_i} \right)$$

where  $u$  is the velocity vector,  $p$  is pressure,  $\rho$  is density, and  $\tau$  is the Reynolds stress tensor. The presented method can be applied not only for

two-dimensional but also for three-dimensional flows (see, for example, [1]).

In the two-dimensional flows the airfoil drag coefficient  $c_x$  can also be calculated from the velocity distribution in the wake behind the model [3,4], measured by a system of velocity field detection from the particle images:

$$c_x = \frac{2}{U_\infty^2 b} \int_W u(U_\infty - u) dy \quad (3)$$

where  $U_\infty$  is the incoming flow velocity,  $u$  is a local velocity in the wake,  $b$  is the model chord, and  $W$  denotes integration along the vertical coordinate in the wake.

## 3 Experimental design, equipment, and procedure

The aim of the study is to evaluate the usability of PIV results to obtain the aerodynamic forces acting on a wing airfoil. For this purpose an experiment was performed in which the airfoil aerodynamic coefficients calculated from the measured velocity fields were compared with similar results obtained by classical methods, by measuring the pressure distribution on the model surface and measuring the total pressure defects in the wake behind the model.

The experiment was performed in a low-speed close-circuit wind tunnel (WT) with an open test section T-03 at TsAGI. The WT has a nozzle of rectangular cross-section area of  $575 \times 370$  mm. The incoming flow velocity was measured with a Pitot-Prandtl tube set at the WT nozzle, and was 30 m/s. A straight wing with a symmetrical airfoil NACA 652-015 was used as a model, with a span of 998 mm and chord length  $b$  of 100 mm, which gives the number of  $Re = 2 \times 10^5$ , calculated from the chord length. The experimental design is presented in Fig. 2. The model was placed horizontally in the center of the WT test section. At zero angle of attack its leading edge was located at a distance of 650 mm from the nozzle exit. The measurements were performed at angles of attack  $\alpha$  of  $0^\circ$ ,  $2.5^\circ$ ,  $5^\circ$ ,  $7.5^\circ$ ,  $10^\circ$ , and  $12.5^\circ$ . The angle of attack was fixed with an accuracy not less than  $0.1^\circ$  by detecting the model end on a video camera. The illumination source provided measurement area in the vertical plane in the

middle of the wingspan. The degree of turbulence in the WT test section (without the model) in the measurement region was 1.3%-1.4%. The velocity coordinate system was used in the studies. The origin of the coordinates was located in the front edge of the model.

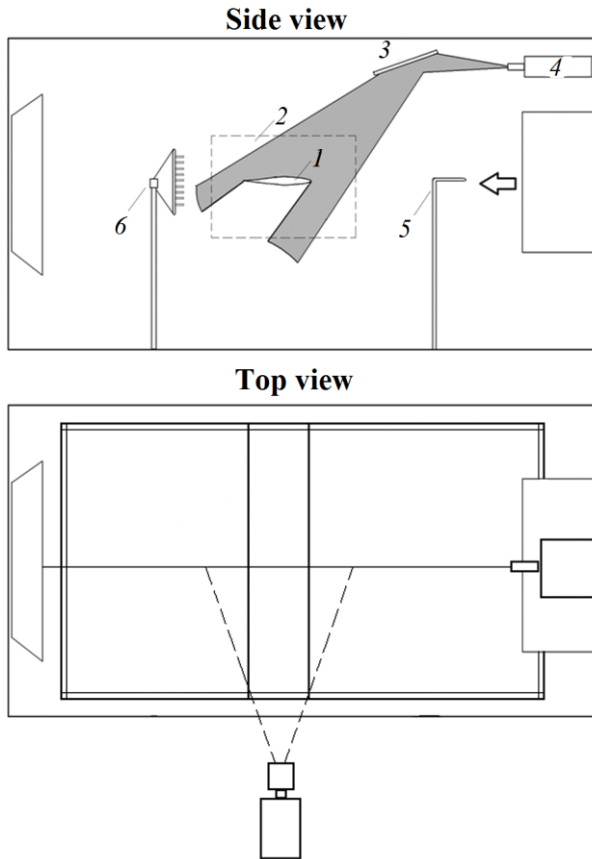


Fig. 2: Experimental design: (1) model; (2) measurement region; (3) mirror; (4) laser; (5) Pitot-Prandtl tube; (6) total pressure rake.

At each angle of attack the loads were measured using PIV and standard methods. The model had 23 pressure taps to measure the pressure distribution over its surface. Since the model was drained only at one side and had a symmetric profile, in order to obtain the surface pressure distribution on both sides of the model the measurements were performed consequently, first at the positive and then at the same negative angle of attack. The lift force was found by integrating the measured surface pressure distributions. The total pressure distribution in the wake behind the model was measured with a total pressure rake, located at the distance of  $1.4b$  from the trailing edge of the model. The nozzles in the rake were spaced with a step of 2.5 mm.

The number of points, describing the total pressure defect in the wake, is 13-15. All sources of pressure signals were connected by flexible pressure tubes to the 32-pressure-sensor container TDM-4. The survey of the sensors was carried out using an I/O subsystem LTR U8, connected to a computer. In order to reduce the effect of the sensor noises in the measurements of pressure distribution on the model surface and in the wake, the averaging by an ensemble of 10-15 samples was performed.

In the present tests the PIV system "POLIS" was used. The layout of the system components is shown in Fig. 2. As a source of tracer particles the aerosol generator Martin MAGNUM 1800 was used. The particle size was  $10 \mu\text{m}$ . The generator was located on the floor of the test section behind the model, so that the smoke was sucked by the flow into the diffuser and returned into the test section passing the entire tube tract. It provided uniform seeding. A double pulse solid-state Nd:YAG laser, Quantel Twins BSL 140, with a wavelength of 532 nm and a pulse energy of 140 mJ served as a source of lighting. The laser sheet thickness in the measurement region was about 2 mm. Cross-correlation camera Videoscanner 4021 (of  $2048 \times 2048$  resolution) and a 50 mm lens allowed fixing an area of  $3.8b \times 3.8b$  size. The laser sheet illuminated the model at the upper side, and the shadow of the model did not allow us to illuminate the entire area around the model by one laser. Therefore, as in the case of pressure measurement, the tests were performed first at the positive, and then at the same negative angle of attack. At each angle of attack 200 frames with 1.25 Hz frequency were recorded, from which the average velocity field was calculated. The average velocity fields obtained at the positive and negative angles of attack were "sewn," which resulted in a complete picture of the flow.

#### 4 Methods of experimental data processing

ActualFlow software was used for image processing [5]. As a result of the application of the iterative cross-correlation algorithm with a continuous shift of regions and 75% overlapping of the calculation regions, we obtained

instantaneous velocity fields with a spatial resolution of  $1.5 \times 1.5$  mm. Statistical processing allowed obtaining of the average velocity fields.

To calculate the derivative of the velocity components a low-frequency filter was used, representing a finite-difference approximation:

$$\left(\frac{\partial f}{\partial x}\right)_i \approx \frac{2f_{i+2} + f_{i+1} - f_{i-1} - 2f_{i-2}}{10\Delta X} \quad (4)$$

This scheme allows distinguishing optimally the low-frequency signal in the presence of uncorrelated noise and is preferable for the regions of 75% overlap [6]. The aerodynamic force calculation was performed for 25 contours in the velocity frame of reference. The distance from the model to the contour of maximum length is  $0.6b - 0.8b$ , depending on the angle of attack. Near the model surface the signal-to-noise ratio is too low due to patches of light that occur when the laser sheet beams reflect on the model surface. Therefore the nearest to the model contour was placed at the distance of  $0.2b - 0.3b$ .

For calculation of pressure along the contour the finite-difference scheme was used:

$$\left(\frac{\partial p}{\partial x}\right)_i = \frac{p_{i+1} - p_i}{\Delta X} \quad (5)$$

The values of the pressure spatial derivatives in the nodes of the computational grid were calculated using formula (1).

The force acting on the airfoil was calculated using formula (2) for each of the contours and was expanded into components  $F_x$  and  $F_y$ . Further, the lift coefficient was calculated:

$$c_y = \frac{2F_y}{\rho U_\infty^2 b} \quad (6)$$

The drag coefficient, defined by momentum conservation law (2), has large errors according to [2] (which is confirmed by the data obtained in the present experiments). Therefore, it was calculated based on the velocity distribution in the wake behind the model, measured by an optical system using formula (3). The calculation was performed for 10 consecutive velocity profiles, located at a distance of  $1.2b - 1.3b$  from the trailing edge of the model. Using the

obtained data the mean value and the measurement error were calculated.

In the present study the accuracy of the aerodynamic force measurement by PIV was determined by comparing the results of measurements of the pressure distribution on the model surface and the total pressure defect in the wake behind it. For this reason, the correct determination of aerodynamic loads from the results of pressure based measurements was given extra attention.

The calculation of the airfoil drag coefficient from the results of the total pressure rake measurements in the wake behind the model was performed using formula [4]:

$$c_x = \frac{2}{b} \int \sqrt{c_p} (1 - \sqrt{c_p}) dY \quad (7)$$

where  $c_p$  is the pressure coefficient measured with the rake. Integration of  $c_p$  distribution along the wake was performed by the trapezoidal method. The nozzle step and their number were quite sufficient to obtain the reliable results, as shown by the present data. Therefore, the errors of the airfoil drag coefficient measurement by this method are determined mainly by the noise of the pressure sensors.

The lift coefficient was found by integrating the measured pressure distributions along the model surface in the body-fixed frame of reference using the standard formula [4]:

$$c_{y1} = \frac{1}{b} \int_0^b (c_p^b - c_p^t) dX \quad (8)$$

and then was recalculated in the velocity frame. Integration was performed using a linear interpolation between the points.

When calculating the lift coefficient from the pressure distributions it has been found that the number of pressure taps near the front edge of the model is not sufficient to obtain the suction peak occurring in this region on NACA type of airfoils at moderate angles of attack. With increasing the angle of attack the extent of this area decreases and the suction peak pressure increases. This leads to a systematic underestimation of the lift force, which can reach 10%. It made it impossible to assess the

accuracy of  $c_y$  calculations from the data of the optical measurements.

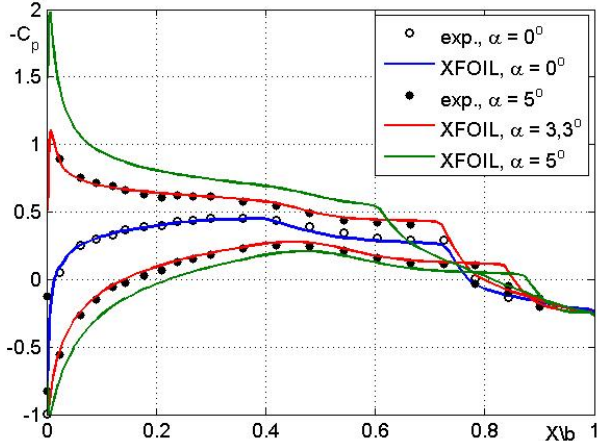


Fig. 3. Comparison of measured and calculated (XFOIL) surface pressure distributions at zero angle of attack,  $Re = 2 \times 10^5$ . Comparison of measured and calculated pressure distributions at  $\alpha = 5^\circ$ ,  $Re = 2 \times 10^5$ , and calculated pressure distribution at  $\alpha = 3.3^\circ$ ,  $Re = 2 \times 10^5$ .

For correction of  $c_y$  the calculated pressure distributions were used, obtained by means of the program XFOIL 6.93 [7], designed to solve the two-dimensional problem of an unlimited flow of a viscous gas around an airfoil. Comparison of the measured and calculated pressure distributions over the airfoil surface at zero angle of attack, presented in Fig. 3, shows a good agreement between the results everywhere except the separation bubble region at  $X/b > 0.6$ , where the correspondence between the results is somewhat worse. With increasing the angle of attack a significant discrepancy between the results is observed (Fig. 3). This is associated with the known phenomenon of reducing the effective angle of attack and decreasing  $c_y$  of wings when tested in a wind tunnel with an open test section, which is caused by two factors: the influence of the free flow boundaries and the appearance of an additional downwash caused by the wing lift force [8,9], which XFOIL is not intended to take into account. In the present paper, this phenomenon is taken into account by carrying out XFOIL calculations for angles of attack in the range from  $0^\circ$  to  $10^\circ$  with a step of  $0.1^\circ$ . From the calculated set of pressure distributions for each of the experimentally studied angles of attack the distribution was

chosen, which most accurately describes the one obtained in the experiment. An example of this is given in Fig. 3, which shows that the experimental distribution at  $\alpha = 5^\circ$  is well approximated by the calculated one at  $\alpha = 3.3^\circ$ .

Since the experiment was performed at a sufficiently low Reynolds number, it was necessary to test the results of XFOIL for airfoil flow at low  $Re$ . To do this, we compared the lift coefficients calculated by XFOIL at  $Re = 2 \times 10^5$  with the results of NACA 652-015 airfoil studies, given in [10] for  $Re = 3 \times 10^6$ . It follows from the data of [10] that up to the angles of attack not less than  $10^\circ$  the lift force of symmetric NACA airfoils of the 6 series is sufficiently well described by a thin airfoil theory (see, e.g., [11], Chap. 5), which gives the following expression for the lift coefficient for an airfoil with a straight midline:

$$c_y = \frac{\pi^2}{90} \alpha \quad (9)$$

where  $\alpha$  has dimensions of degrees. Comparison of the data presented in [10] for airfoil NACA652-015 with the calculation and the thin airfoil theory is shown in Fig. 4. As seen from the figure, at  $Re = 2 \times 10^5$  XFOIL results are in good agreement with the thin airfoil theory up to the angle of attack of  $5^\circ$ , after which there is a significant discrepancy in data. Therefore, in this study the calculated pressure distributions were used only for the calculation of  $c_y$  amendments at the experimentally investigated angles of attack of  $2.5^\circ$ ,  $5^\circ$ , and  $7.5^\circ$ .

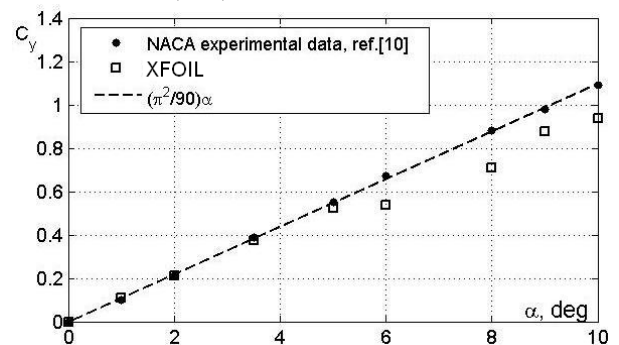


Fig. 4. Comparison of the experimental ([10],  $Re = 3 \times 10^6$ ) and calculated (XFOIL,  $Re = 2 \times 10^5$ )  $c_y$  dependences on the angle of attack; (dashed line) the dependence for symmetric airfoils given by the thin airfoil theory.

The procedure for amendment calculation is illustrated in Fig. 5. The pressure coefficients were taken on the calculated curves at the pressure taps coordinates, and the lift coefficient was calculated by integrating this selective dependence at  $X/b < 0.5$ , using the same linear interpolation procedure as in the integration of experimental distributions. The difference in the integrals obtained from the full and selective  $c_p(X/b)$  dependencies, shown in Fig. 5 in the form of a dark-filled area, gives the probable underestimation of the lift force when measuring it experimentally based on the surface pressure distribution on the airfoil. The amendments obtain this way are presented below in absolute values. They increase with increasing  $\alpha$ , since in this case the suction peak becomes more pronounced. The corrected  $c_y$  values were obtained by adding the corresponding amendments to the coefficients calculated from the experimental pressure distributions.

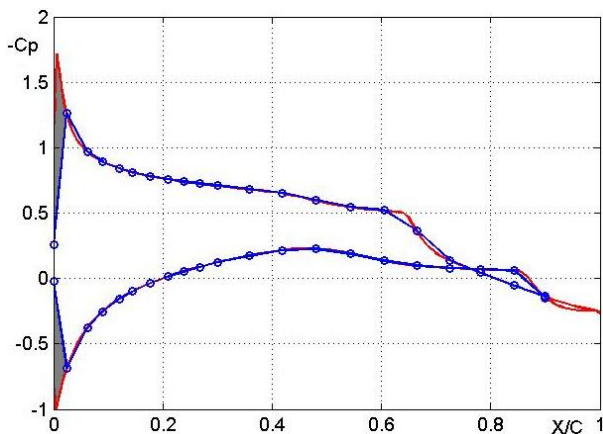


Fig. 5. Calculated pressure distribution at  $\alpha = 4.5^\circ$ ,  $Re = 2 \times 10^5$ : (open circles) selective dependence  $c_p(X/b)$ , plotted from the location coordinates of the pressure taps; (shaded area) region of the suction peak, where amendments for  $c_y^{pr}$ , obtained from the experimental data for  $\alpha = 7.5^\circ$ , were calculated.

## 5 Experimental results

Figure 6 shows an example of a velocity absolute value field obtained in the experiment at the angle of attack  $5^\circ$ , and also the streamlines constructed from the measured velocity vectors. Field regions near the model contain false velocity vectors due to various optical interferences (mainly flare spots while reflecting

the laser sheet from the surface), which are not shown in the figure. However, it is important to note here that the regions of the velocity field

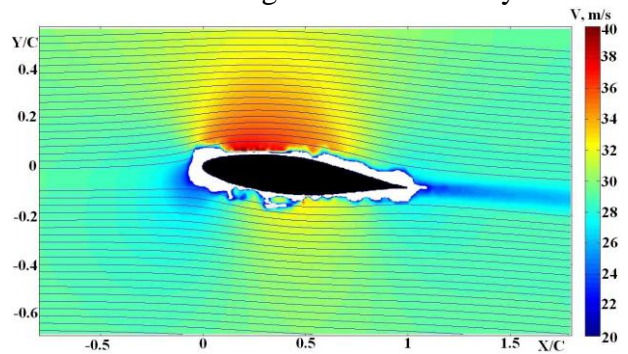


Fig. 6. The absolute velocity field, measured with the PIV system and the streamlines pattern at  $\alpha = 5^\circ$ .

measured at a sufficiently large distance from the model more than  $0.2b$  both in the longitudinal and vertical direction are of the greatest meaning for the method under consideration. In these flow field regions the obtained results agree well with the known views about the features of two-dimensional airfoil flow. In particular, one can notice the flow deceleration near the nozzle of the model, slight flow acceleration on the airfoil windward side and its greater acceleration on the leeward side, and also in the wake behind the model.

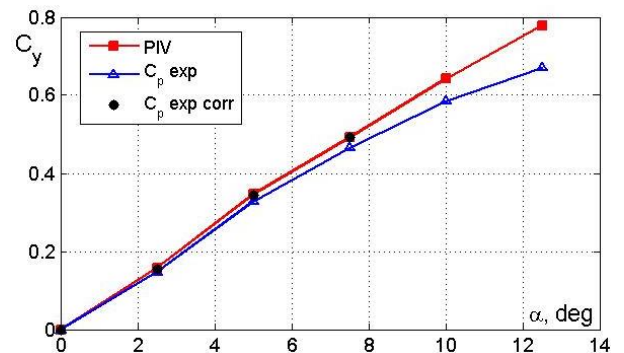


Fig. 7. Comparison of  $c_y$  dependences on the angle of attack, defined from the PIV data, pressure distribution, and the corrected one in the range of  $\alpha$  up to  $7.5^\circ$  taking into account the correction in the suction peak.

The lift coefficients, calculated from the measured velocity fields and the surface pressure distribution on the model are shown in Fig. 7. For the optical method the mean  $c_y$  values are presented, obtained by averaging the calculation

results for 25 control contours. It can be mentioned that  $c_y$  coefficients calculated from the pressure distribution are always lower than those calculated based on the optical system

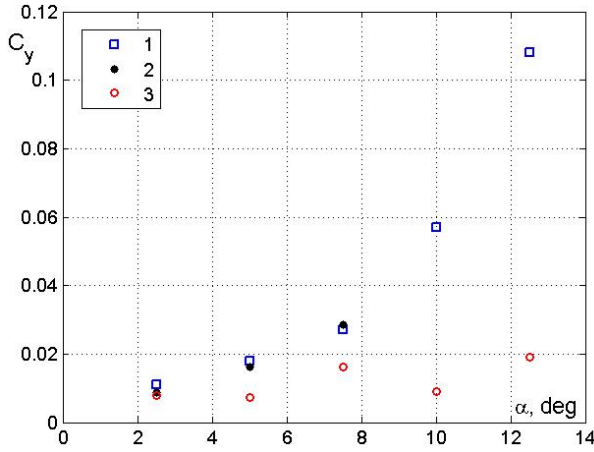


Fig. 8. Error absolute values in  $c_y$  determination versus the angle of attack: 1 - difference  $c_y^{PIV} - c_y^{pr}$ ; 2 - calculated  $c_y$  amendment in the suction peak; 3 - doubled standard deviation of  $c_y$  from the PIV system.

data. Dependence  $c_y(\alpha)$ , obtained by the optical method, is much closer to a straight line over the entire range of angles of attack than the dependence obtained by integrating pressure. The difference between coefficients  $c_y$ , calculated in two ways, is shown in Fig. 8. It is evident that this difference increases by an order with increasing the angle of attack. The relative difference increases from 6% to 7% at low angles of attack up to 14% at  $\alpha = 12.5^\circ$  (Fig. 9). However, the analysis of pressure distribution on the model surface performed by XFOIL using the described above procedure shows that these differences are caused by the features of the surface pressure distribution measurements for determining  $c_y$  and cannot be used to assess the accuracy of the optical method. As has been indicated before, when increasing the angle of attack, the suction peak in the surface pressure distribution near the leading edge becomes more pronounced, which could not be correctly measured at the given distribution of pressure receivers on the model. The amendments for the lift coefficients determined from the pressure based measurements, calculated using XFOIL data in the suction peak, are also shown in Fig. 8 for the angles of attack up to  $7.5^\circ$ . As follows

from the figure, the magnitudes of these amendments are almost equal to the residual obtained when comparing the two methods of measurement. The corrected values of  $c_y$  are shown in Fig. 7 for angles of attack  $2.5^\circ$ ,  $5^\circ$ , and  $7.5^\circ$ . One can see a good agreement of corrected coefficients with the ones, calculated from the optical method data. The relative residual here does not increase 2% at  $\alpha = 2.5^\circ$  and is less than 1% at  $\alpha = 5^\circ$  and  $7.5^\circ$ .

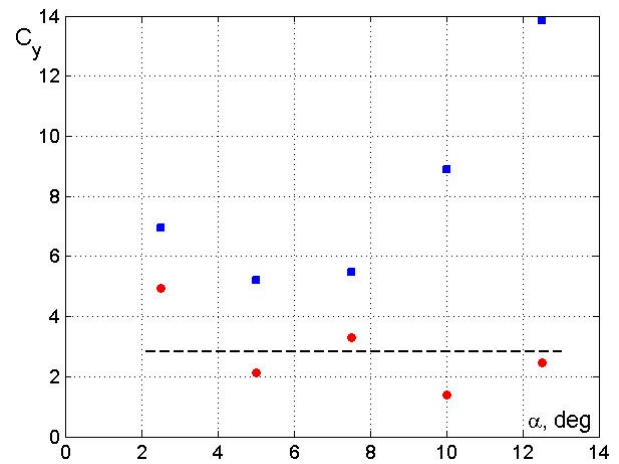


Fig. 9. Relative errors in  $c_y$  determination versus the angle of attack: (blue squares) value  $(c_y^{PIV} - c_y^{pr}) / c_y^{PIV}$ ; (red circles) doubled standard deviation of  $c_y$  from the PIV system; (dashed line) mean value of the doubled standard deviation from PIV data, equaling 2.83%.

The results presented above show that the lift coefficient can be measured by an optical nonintrusive method with an accuracy sufficient for many applications. The measurement error can be determined from the scatter of the computation results for the contours, spaced from the model at various distances. Absolute values of the doubled standard deviation from the mean obtained for the 25 contours are shown in Fig. 8 depending on the angle of attack. They do not exceed 0.02. Dependence of the relative doubled standard deviation (i.e., related to the corresponding mean value) on the angle of attack is shown in Fig. 9. This value decreases somehow with increasing  $\alpha$ , from 5% to 2%. Its mean value for the entire set of data is 2.83%. Thus, it can be concluded from the presented data that the lift coefficient can be measured by an optical nonintrusive method using the system

of velocity field detection from the particle images with an error not exceeding 3%.

Figure 10 shows the results of the two methods of measuring the drag coefficient. The wake rake and optical measurements data are in sufficiently good agreement, although  $c_x$  values obtained by the optical method are slightly higher than those obtained using the total pressure rake. The residual absolute value was almost constant over the entire studied range of angles of attack and was  $\sim 0.001$ . The relative residual value is no more than 1.5% in the range of angles of attack  $7.5^\circ - 12.5^\circ$ , increasing at low angles of attack, up to 6%. The mean value of the relative residual over the entire studied range of angles of attack was 3.2%. The doubled standard deviations obtained from 10 samplings of the total pressure defect, or from 10 consecutive profiles of velocity defect in the wake when using the optical method, were shown in the figure as the error bars. As one can see in Fig. 10, the ranges of  $c_x$  values, in which fall 95% of the measurement results by one or another method, always overlap. It should be mentioned that the scatter of  $c_x$  calculated from the optical system data is comparable to scatter obtained in wake rake measurements, and is significantly less at high angles of attack. The results obtained thus show that the drag coefficient as well as the lift coefficient can be measured by an optical nonintrusive method with an error of about 3%.

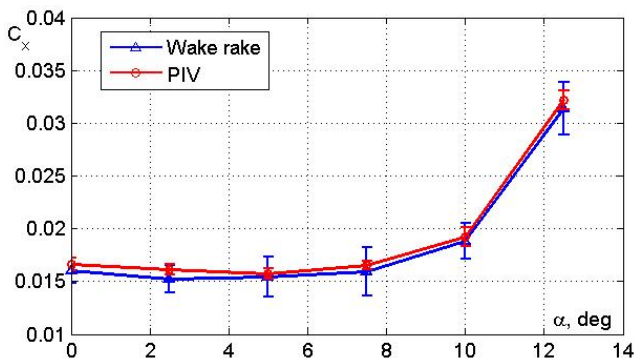


Fig. 10. Comparison of  $c_x$  dependences on the angle of attack, defined from the total pressure defect in the wake and the PIV system data.

The given data allow one to conclude that using the complex of velocity field detection from the particle images "POLIS" provides a

definition of the aerodynamic coefficients for two-dimensional flow around a wing airfoil with an average error no more than 3%-3.2%.

## 6 Conclusions

The method of determining the aerodynamic forces acting on an airfoil in the flow at low Reynolds numbers from the velocity field measured with PIV is considered. Lift and drag forces can be obtained by integrating the gas dynamic characteristics of the flow along the contour around an airfoil (the control volume method). The drag coefficient can also be calculated by the velocity defect in the wake behind the model.

The results of PIV measurements were compared to the results of pressure based measurements (the pressure distribution on the model surface and the total pressure defect in the wake behind the model). The comparison showed good agreement between the measurement results of the lift coefficient by the control volume method and by pressure distribution over the model surface. The relative residual here is less than 2% at angles of attack up to  $10^\circ$ . Analysis of the measurement results showed that the drag coefficient calculation based on the velocity defect in the wake gives a more reasonable result compared to the control volume calculation. The average residual with the results of total pressure defect measurement in the wake is less than 3.2%. The error of lift and drag force measurement by the PIV system was less than 3.5%.

## References

- [1] Berton, E., Maresca, C., and Favier, D., A new experimental method for determining local airloads on rotor blades in forward flight, *Exp. Fluids*, Vol. 37, No. 3, pp. 455-457, 2004.
- [2] Van Oudheusden, B. W., Casimiri, E. W. F., and Scarano, F., Aerodynamic load characterisation of a low speed aerofoil using particle image velocimetry, *Aeronaut. J.*, Vol. 112, No.1130, pp. 197-205, 2008.
- [3] Schlichting, G., *Boundary-Layer Theory*, Moscow: Nauka, 1974 (in Russian).
- [4] Martynov, A. K., *Applied Aerodynamics*, Moscow: Mashinostroenie, 1972 (in Russian).
- [5] License of POLIS enterprise for Actual Flow Software no. 25497C20.

- [6] Raffel, M., Willert, C., and Kompenhans, J., *Particle Image Velocimetry. A Practical Guide*, Berlin: Springer, 1998.
- [7] Drela, M. and Giles, M. B., Viscous-inviscid analysis of transonic and low Reynolds number airfoils, *AIAA J.*, Vol. 25, No. 10, pp. 1347-1355, 1987.
- [8] Yuryev, B. N., *Experimental Aerodynamics*, Vol. 2. Moscow, Leningrad: Izd. narkom. oboron. prom., 1938 (in Russian).
- [9] Carafoli, E., *Aerodynamics of Airfoil Wings*, Moscow: Izd. Akad. Nauk USSR, 1956 (in Russian).
- [10] Abbott, I. H., von Doenhoff, A. E, and Stivers, Jr., L., Summary of airfoil data, *NACA TR-824*, 1945.
- [11] Loytsyanskiy, L. G., *Mechanics of Liquid and Gas*, Moscow: Nauka, 1978 (in Russian).

**7 Contact Author Email Address:**  
**Gadji\_@mail.ru**

### **Copyright Statement**

The authors confirm that they, and/or their company or organization, hold copyright on all of the original material included in this paper. The authors also confirm that they have obtained permission, from the copyright holder of any third party material included in this paper, to publish it as part of their paper. The authors confirm that they give permission, or have obtained permission from the copyright holder of this paper, for the publication and distribution of this paper as part of the ICAS 2014 proceedings or as individual off-prints from the proceedings.